

Advanced Digital-SCAL measurements of gas trapped in sandstone

Ying Gao^{1,3,*}, Tibi Sorop¹, Niels Brussee¹, Hilbert van der Linde¹, Ab Coorn¹, Matthias Appel² and Steffen Berg^{1,3,4}

¹Shell Global Solutions International B.V., Grasweg 31, 1031 HW Amsterdam, Netherlands

²Shell International Exploration and Production Inc., 3333 Highway 6 S, Houston, TX 77082, USA

³Imperial College London, Department of Earth Science & Engineering, Exhibition Rd, South Kensington, London SW7 2BX, United Kingdom

⁴Imperial College London, Department of Chemical Engineering, Exhibition Rd, South Kensington, London SW7 2BX, United Kingdom

Abstract. Trapped gas saturation (S_{gr}) plays an important role in subsurface engineering such as carbon capture and storage, H_2 storage efficiency as well as the production of natural gas. Unfortunately, S_{gr} is notoriously difficult to measure in the laboratory or field. The conventional method of measurement- low-rate unsteady-state core flooding - is often impacted by gas dissolution effects, resulting in large uncertainties of the measured S_{gr} . Moreover, it is not understood why this effect occurs even for brines carefully pre-equilibrated with gas. In order to address this question, we used high resolution X-ray CT imaging techniques to directly visualize the pore-scale processes during gas trapping. Consistent with previous studies we find that for pre-equilibrated brine, the remaining gas saturation continually decreased with more (pre-equilibrated) brine injected and even after the brine injection was stopped, resulting in very low S_{gr} values (possibly even zero) at the pore scale level. Furthermore, we were able to clearly observe the initial trapping of gas by snap-off effect followed by a further shrinkage of the gas clusters that had no connected pathway to the outside. Our experimental insights suggest that the effect is related to the effective phase behaviour of gas inside the porous medium which due to the geometric confinement could be different than the phase behaviour of bulk fluids. The underlying mechanism is likely linked to ripening dynamics which involves a coupling between phase equilibrium and dissolution/partitioning of components, diffusive transport and capillarity in the geometric confinement of the pore space.

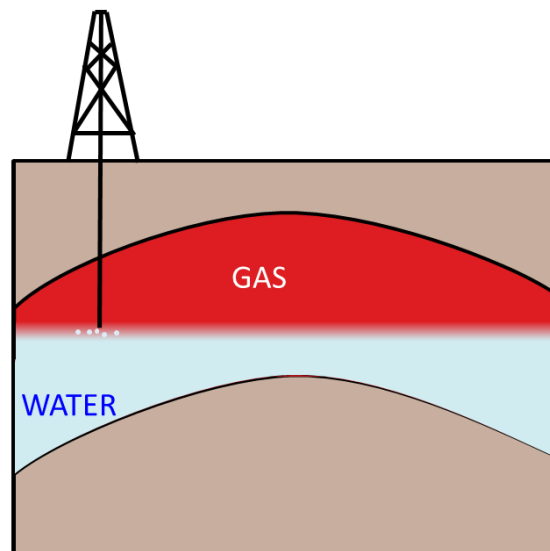
1 Introduction

In the space of multiphase flow in porous media which is encountered in many industrial surface and sub-surface applications such as groundwater management, contaminant hydrology and hydrocarbon recovery the recent focus on climate change and energy transition is also putting a higher priority on subsurface process that involve gasses such as carbon dioxide sequestration (CCS) and underground hydrogen storage [1-4]. For the gas-related processes ranging from natural gas production to CCS and H_2 storage, the trapped gas saturation (S_{gr}) is a key parameter [5-7].

Natural gas is mainly produced from gas reservoirs by pressure depletion. During production the reservoir pore pressure decreases. If a strong aquifer is present, the free water level could then rise during production because of the pressure depletion, causing the water from aquifer to imbibe into the pore space previously filled by gas (as rock in gas reservoirs is predominantly water-wet due to the absence of longer-chain hydrocarbon components), as sketched in Fig. 1. Water imbibition will then lead to capillary trapping of gas and limit the fraction of gas that can be produced, and hence negatively impact the economics of the projects. Similar considerations apply to hydrogen storage and CO_2

sequestration for which the amount of trapping can lead to different storage volumes than otherwise expected.

The trapped gas saturation depends on several parameters ranging from the phase behaviour/pressure-temperature conditions, depletion rate, rock type, wettability and interfacial tensions, and other petrophysical properties (porosity, permeability) to initial gas saturation [5-10].



* Corresponding author: Y.Gao3@shell.com

Fig. 1. Schematics of a gas reservoir with one producing well by pressure depletion, for the case of an active aquifer.

In practice, trapped gas saturations need to be measured experimentally. The importance of core analysis measurements for determination of residual gas saturation has long been recognised and a large amount of experimental work has been conducted in industry. Residual gas saturations reported in the literature range from 5% to 60% for the same porosity and for similar initial water saturations (there are reports suggesting even more than 70%, for tight samples) [11-22]. While it is known that residual saturation does not only depend on average porosity but also the pore structure, this large variation still raises the question whether this very large variation is not caused by other effects. This question was addressed in the study by Cense et al. [6] using one-dimensional in-situ X-ray saturation monitoring (ISSM) in USS core flooding experiments. It was observed that gas starts to dissolve within the core near the inlet while still gas is still displaced at outlet i.e. before trapping was reached [6] even though the injected brine was carefully pre-saturated with gas. That basically means that before reaching a true residual saturation (without any further gas displacement) the dissolution at the inlet may prevent or hide establishing a clear residual gas saturation over the whole sample [5-7] which would negatively impact the reliability of such measurements.

The advancement of pore scale imaging capability by X-ray computed micro tomography [26-27] provides an opportunity to investigate this problem in more detail. The micro-CT technology can provide not only the measurements of porosity, permeability, saturation of different phases, relative permeability, but also characterize the dynamics of gas/oil/water systems inside complex pore geometries at the scale of individual trapped gas bubbles [26,28]. This means that the trapping dynamics can now be visualised at the pore scale [35-40]. Iglauer et al. [41] started to image the trapped gas at the pore scale in a sandstone. Then Chaudhary et al. [42] extended the trapped CO₂ in various bead packs with wettability. Andrew et al. [43,44] imaged the trapped CO₂ in sandstone and carbonate under in-situ reservoir conditions. Furthermore, in addition to the long static images, dynamic imaging capability brings more advantage on study unsteady-state flow [28-34]. However, there has been no dynamic study on trapped gas saturation to learn why the uncertainty of the measured S_{gr} at core scale is so large.

The aim of this study is to address this question and quantify trapped gas saturation in sandstone rock by performing core flooding experiments with *dynamic* imaging by micro-CT which has been successfully applied in the past for studying the dynamic behaviour of the non-wetting phase [28,29,33] and gas [45,46]. In order to understand the reason why trapped gas dissolves despite the brine being saturated, which is one of the causes for the large range of observe S_{gr} , we conducted core flooding experiments with both gas saturated brine and unsaturated brine with dynamic imaging and establish the differences in flow regimes and compare the difference in dissolution characteristics.

2 Materials and methods

2.1. Rock samples and fluid properties

A cylindrical sample of a Bentheimer sandstone with the diameter of 4 mm and length of 20 mm was used in this study, see Fig. 2. The porosity estimated from the micro-CT image was 20.4 %, more details could be found in Section 2.3.2. The permeability measured on the bulk plug, where this mini-plug was drilled, is $2.48 \times 10^{-12} \text{ m}^2$.

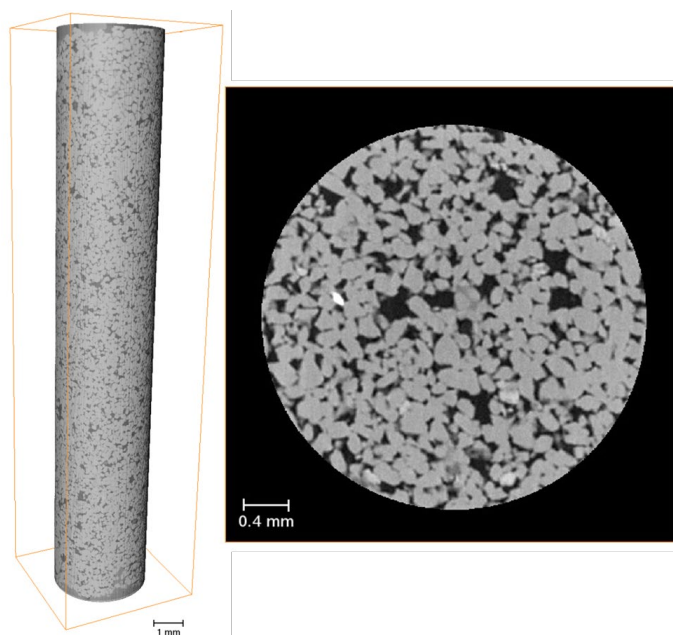


Fig. 2. On the left, three-dimensional X-ray image of the whole sample used in the experiment, with voxel size of 5 μm . On the right, two-dimensional cross sections of three-dimensional micro-CT images of a dry scan. The dark is pore space and the grey is grain.

The brine used in this study is water doped with 5 wt% NaI to increase the contrast and to distinguish the interface between gas and brine. The gas used in this work is compressed air.

2.2 Experimental methods

Unsteady state (USS) brine displacing gas experiments at laboratory temperature were conducted. This study consisted of two main experiments: a) an USS flow experiment performed using the gas saturated brine at 0.5 $\mu\text{L}/\text{min}$; and b) an USS flow experiment performed using unsaturated brine at 0.5 $\mu\text{L}/\text{min}$. From these two experiments, we could compare how gas dissolution impact the trapped gas saturation.

The flow apparatus of these experiments is shown in Fig. 3. The experimental flow apparatus showing the three main components: core holder, differential pressure transducer, and four syringe pumps to apply a constant flow rate as well as confining and back pressure. The sample was placed in a fluoropolymer elastomer (Viton) sleeve in the carbon fibre

Hassler type flow cell. Fluid flow lines were used to connect the core holder with the pumps. The core holder used in this work is shown in Fig. 4.

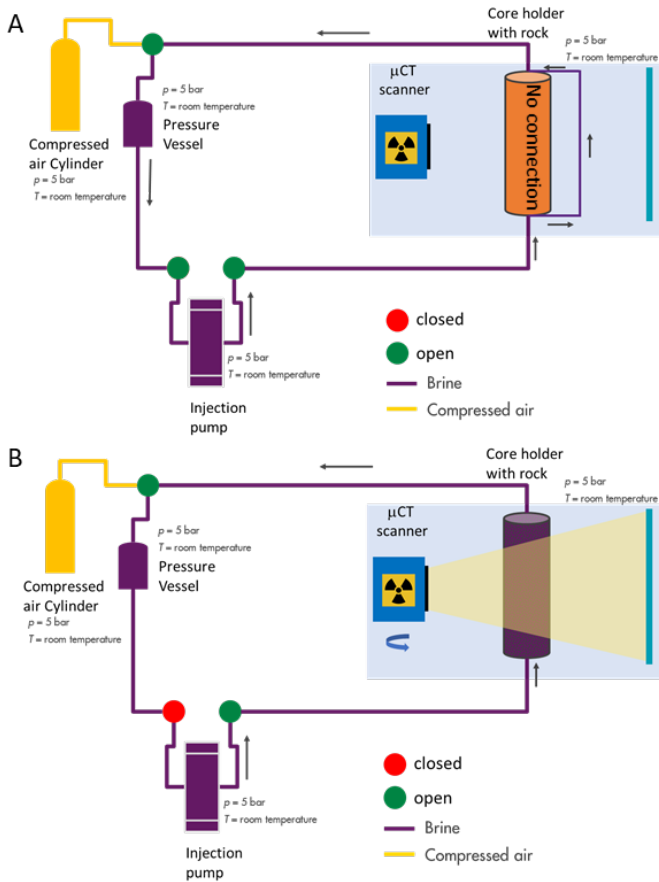


Fig. 3. The experimental flow apparatus used in this work: (A) for mixing brine and compressed air; (B) for displacement experiments.

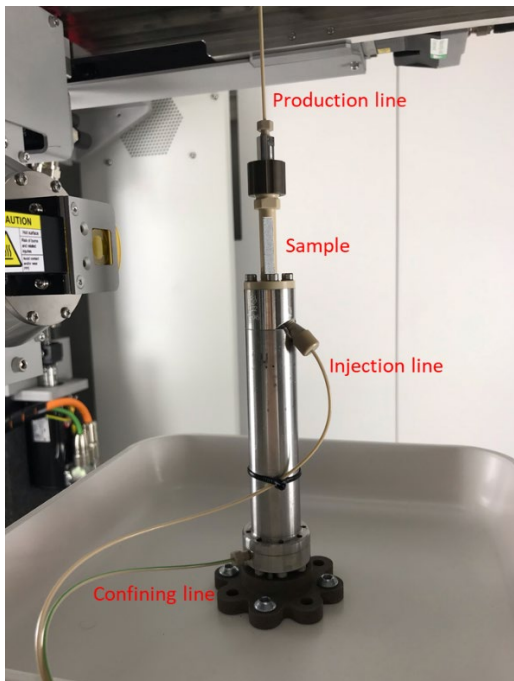


Fig. 4. The core holder used in this study. Brine was injected from the bottom of the sample and the production line is at the top of the core holder.

The experiments were performed by following the steps:

1. The brine was prepared in the Quizix pump at 5 bar.
2. The Bentheimer rock sample was put in the Viton sleeve in the core holder. Fluid flow lines were used to connect the pumps and core holder that was mounted inside the micro-CT scanner.
3. Confining pressure was applied by injecting deionized water into the empty annulus space between the carbon fibre sleeve and the Viton sleeve. To avoid any bypass flow between the sample and the sleeve, the confining pressure was set as 30 bar.
4. A dry scan of the whole sample was taken with the voxel size of 5 μm .
5. The back pressure was set at 5 bar using water saturated compressed air.
6. Brine and compressed air were mixed by recirculating through the flow lines bypassing the sample at 5 bar for more than 48 hours, as Fig. 3(A) shows. The compressed air cylinder was open and the sample was disconnected from the flow line.
7. Only air was inside of the rock sample at the start of the experiment, meaning that the initial gas saturation is 1. Brine was injected at a very low flow rate of 0.5 $\mu\text{L}/\text{min}$ to ensure that the pressure drop across the sample is less than 2% of the pore pressure (as recommended in [6]) to make sure that the pressure gradient along the sample would not be too high to dissolve more compressed air. The pressure drop along the sample would be from 0.6 mbar when it was fully saturated with brine, which is far more less than 5 bar – the back pressure. Fig. 3(B) shows the flow loop for the displacement experiments.
8. Images with voxel size of 5 μm were taken at the same time continually during the coreflooding. It usually takes around 30 minutes for a high-resolution 3D image.

For the first experiment – (USS coreflood performed using the gas saturated brine) we found that after breakthrough the gas saturation changes slowly if we keep injecting beyond 1 PV. At this stage of the experiment, the images were taken once every hour. After injecting 32 PV, the flow rate was increased to 1 $\mu\text{L}/\text{min}$ and then to 2 $\mu\text{L}/\text{min}$ after injecting 46 PV. The experiment was stopped when no gas was found in the sample, after around 60 hours.

For the second experiment – (USS flow experiment performed using the unsaturated brine) we follow a similar protocol, however since we found that all the gas in the sample disappeared after injecting 4 PV, we stopped the tests after around 5 hours.

2.3 Imaging methods and processing

2.3.1 Imaging Method

The 3D images were taken by a TESCAN DynaTOM X-ray microscope (which is a vertical gantry based micro-CT) using a flat panel detector, see Fig. 5. The X-ray energy was 130

keV and the power was 16 W. The number of projections for the dry scan was 2200 and the average of the frame was 10 to enhance image quality and the projections of the dynamic scans was 1500 with 1 frame averaging. There are two key advantages of this scanner when flow experiments were conducted: (1) the gantry rotates 360 degrees with sample fixed on the sample stage without moving the flow lines - keeping the stability of the core flooding experiment, (2) the time resolution for imaging is very quick, so it only takes 30 minutes to take the image of the whole sample length (which was scanned in 4 segments) compared to several hours for a conventional desktop micro-CT scanner for only one segment.

All tomograms were reconstructed into three-dimensional images using the Panteha reconstruction software (TESCAN). The voxel size of all the images is 5 μm and the size of the images was 800 \times 800 \times 3780.

All images were registered to the dry scan to have the same orientation. The Lanczos algorithm was used to resample the images [46]. A non-local means filter was used to remove noise and smooth the images while preserving edges [48-50].

The images are processed in Avizo using the watershed method for segmentation.

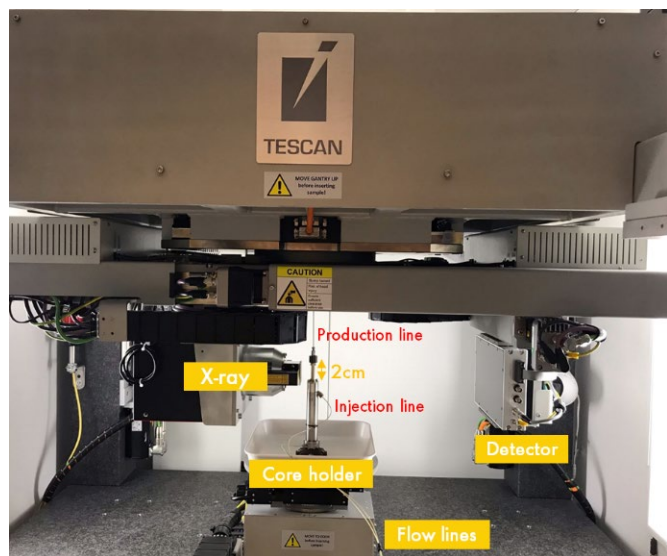


Fig. 5. Flow apparatus placed inside the gantry of the DynaTOM micro-CT scanner.

2.3.2 Characterization of the fluid in the pore space

The cross-section images of the sample are shown in Fig. 6. The top image shows the segmented image of the dry scan, pore space in blue and grains in grey. The bottom image shows the segmented image when 25.6 PV brine was injected, with brine in blue, gas in red and grains in grey.

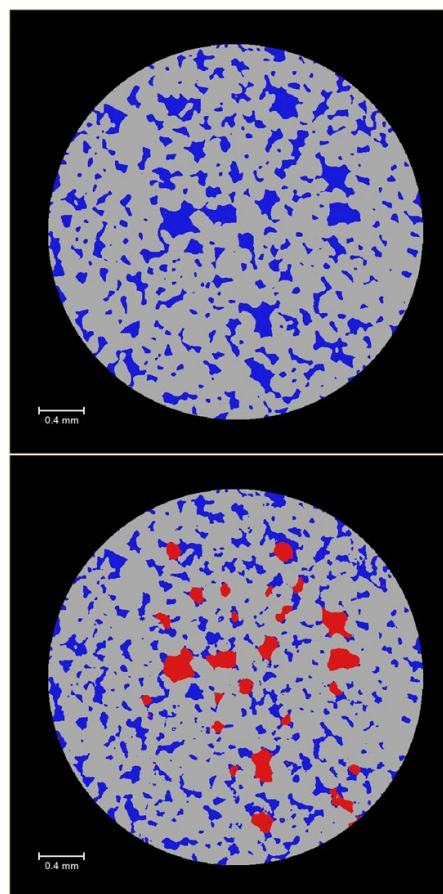


Fig. 6. Two-dimensional cross sections (same slice as in Fig. 2) of three-dimensional segmented images of a dry scan (top). At the bottom we show the same slice for a flow experiment with the gas phase in red and brine in blue.

3 Results and discussion

In the Section 3.1 and Section 3.2 respectively, we present the trapped gas distribution and the quantification of the gas saturation across the sample for the two USS experiments described in the previous section. This is followed by the comparison and discussion of these two experiments: in Section 3.3 on saturation profiles and in Section 3.4 on how trapped gas distributes through the inner pore space.

3.1. USS flow experiment with gas saturated brine

The USS flow experiment using gas saturated brine was performed in 60.1 hours during which 30 whole-sample 3D images were collected. Fig. 7 shows a time sequence with 10 representative examples taken at different stages, displaying the water/gas displacement process. As expected, we found that the brine has invaded the whole sample relatively quickly, aided by the spontaneous imbibition process. As a result, quickly after breakthrough, the gas in the pore throats was displaced leaving ultimately trapped gas in the large pore bodies. If we continue injection, we find however that after about 8 PV injected, the gas completely disappeared first near the inlet of the sample then gradually more gas disappeared from the inlet to the outlet. At the end of the process, if we continue injecting even more brine all of the gas from the sample disappeared.

To quantify the gas saturation at each pore volume injected, images were all segmented using interactive thresholding module in the Avizo software. Fig. 8 shows the average gas saturation in the sample as a function of pore volume injected, as a red curve. Three stages can be identified. For the first stage (from 0 to 1-2 PV) the water/gas displacement process plays a dominant role. We infer this from the gradient of saturation vs. injected volume curve ~ 0.96 , which is very close to 1. Gas saturation decreased from 1 to around 0.38 during the injection of the first PV of brine. For the next two stages we hypothesize that even though we carefully prepared and saturated the brine with gas, the gas-brine dissolution plays an important role. In the second stage (2 to 18 PV injected) a decrease in S_g from 0.38 to 0.1 is observed. We label this as the first stage of dissolution (i.e. Dissolution 1). Next, the dissolution rate decreased to a lower rate (which we label as Dissolution 2) until there is no gas in the pores and throats. Thus, even though the brine was fully saturated with gas before the start of the experiment, gas could still dissolve slowly in the brine. As less and less gas-brine interfaces are available when more PV brine was injected, the dissolution rate decreased leading to two dissolution regimes each with constant dissolution rate (linear decrease of gas saturation with time). At this point it is not entirely clear what these two different regimes represent but it is possible that the Dissolution 1 regime might still contain some displacement (and hence saturation decreases faster) while the Dissolution 2 regime contains only dissolution.

3.2. USS flow experiment with unsaturated brine

At the moment of performing the first tests it was not clear what really causes the dissolution of the gas, even though the injection brine is gas saturated. In order to get a clear reference point to what conventional dissolution would look-like, we performed a second experiment in which we injected unsaturated brine.

This experiment lasted 5.3 hours and 10 images were collected. Fig. 9 shows how gas distributes when more unsaturated brine was injected. Grey-scale images show how gas was displaced.

Fig. 10 shows the gas saturation as a function of pore volume injected. Compared with the USS flow experiments with fully saturated brine (in Section 3.1), we only see two stages in this experiment. Consistent with the first experiment, S_{gr} decreased from 1 to 0.17 when 1.5 PV brine was injected, in which displacement dominated the change on S_{gr} . It is not always possible to completely distinguish the proportion of displacement and dissolution. But when looking at Fig. 11 and 12 it is clear that saturation increase beyond $1-S_{gr}$ has to be dissolution, where S_{gr} is typically in the range of 10% or more, depending on a number of parameters. So saturations close to 100% brine would mean that some dissolution has to have happened. On the other hand, while gas is still connected as visible from the connectivity in Fig. 13 and 14, displacement is the faster process. The discrimination is perhaps best done when looking at the average gas saturation vs. injected PV in Figs. 8 and 10, where we can relate regions

if similar slope with the intervals in Fig. 11 - 14 where we can identify the dominant mechanism. As the absolute value of the gradient of this curve is 0.75, not only displacement, but also the dissolution plays a role on saturation change. Then the S_{gr} decreased to 0 in 3 hours in a very low dissolution rate. However, the dissolution stage starts at earlier stage than the experiment with saturated brine and the displacement and dissolution happened at the same time, as indicated in Fig. 10.

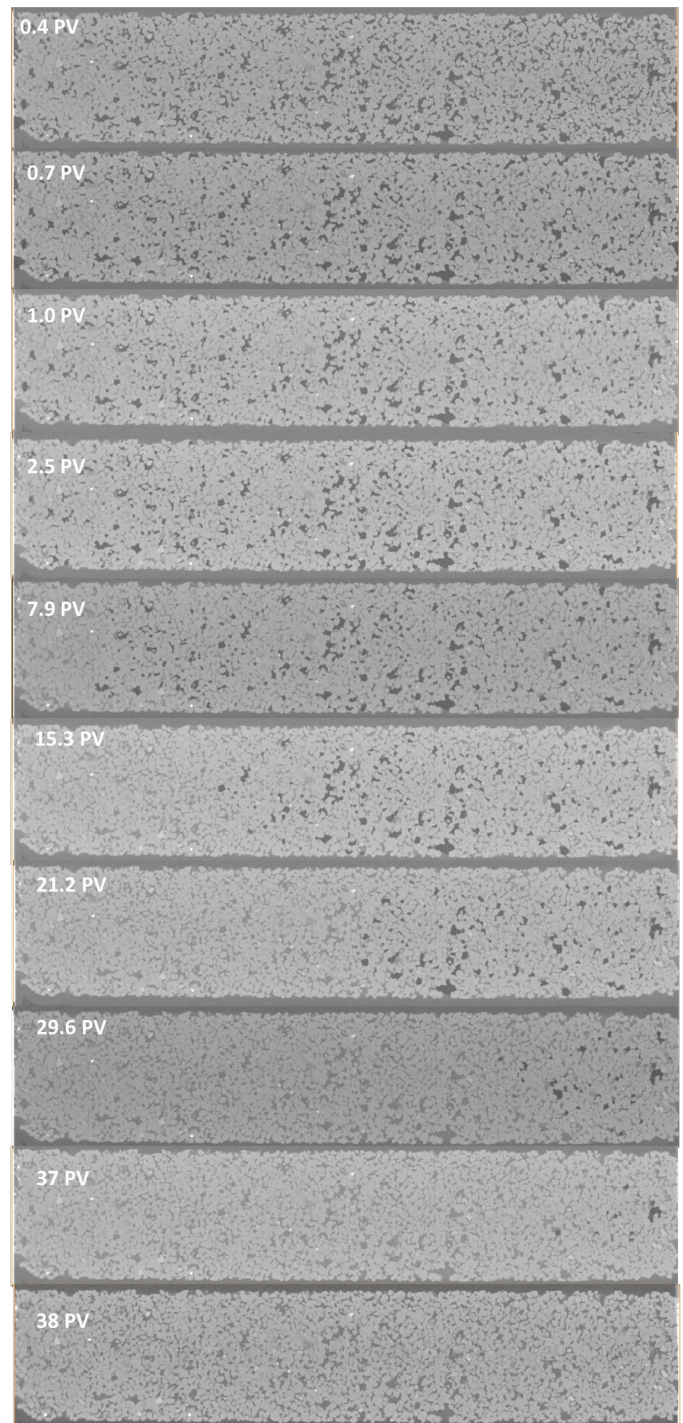


Fig. 7. 2D grey-scale images perpendicular to the flow direction when the sample was flooded by the gas saturated brine. The

injection direction is from left to right. Light grey is grain, dark grey is brine, and the black is gas.

by a combination of interfacial area but also solute dispersion in combination with local thermodynamics and dissolution kinetics which should also scale somehow with factors such as local capillary pressure in the gas bubble and local (super) saturation in the brine.

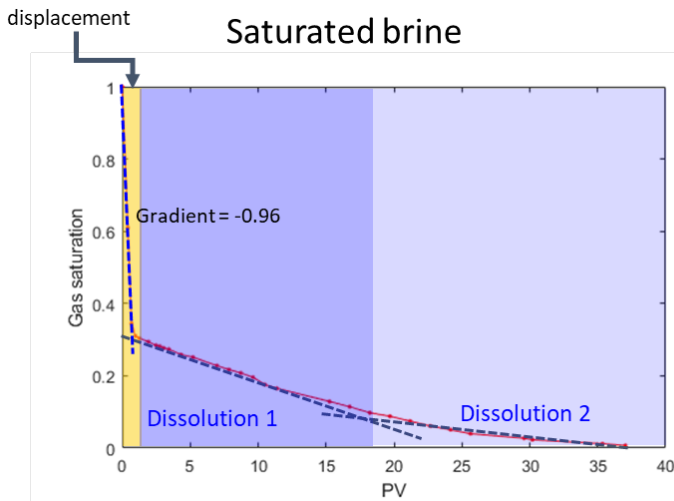


Fig. 8. For the USS flow experiment with gas saturated brine, the red curve shows the trapped saturations as a function of pore volumes injected. The yellow shadow is displacement stage, dark purple represents the “Dissolution 1” stage and light purple represents the “Dissolution 2” stage.

3.3. Saturation profiles

In order to get further insights, the saturation profiles along the cores were computed for the two experiments from Fig. 7 and Fig. 9. From the segmented 3D images the saturation in each slice perpendicular to the long sample axis was averaged and plotted vs. distance from the inlet. The respective saturation profiles shown in Fig. 11 and Fig. 12 illustrate the trend how the gas distributes in the whole sample when injecting saturated and un-saturated brine, respectively.

In Fig. 11, we can see the brine has imbibed into a lot of small pores and throats during the injection of 1-2 PV leading to significant trapping, which is related to the Displacement stage. Then the brine saturation increases throughout the sample in a homogeneous manner, which is a signature for displacement processes. At some point the gas phase starts to disappear from the inlet above the trapping limit at the stage of Dissolution 1 i.e. as a frontal dissolution process. However, we still see some homogeneous increase of saturation during that stage in a similar manner as during the displacement stage which could indicate that during this stage still displacement occurs. Then the Dissolution 2 starts until S_{gr} locally decreases to 0.

Because of the involvement of many parameters in particular the solute dispersion behaviour, and the proportionality to the interfacial area, the dissolution rate limit is not so easy to estimate. At equilibrium, the gas dissolution limit in unsaturated brine at 5 bar is about 2 vol%. But the actual dissolution rate, which could be calculated from the saturation change from Fig. 8 and 10, exceeds the equilibrium assumption, which means that such simple estimates do not work. We think that at the end the dissolution rate is governed

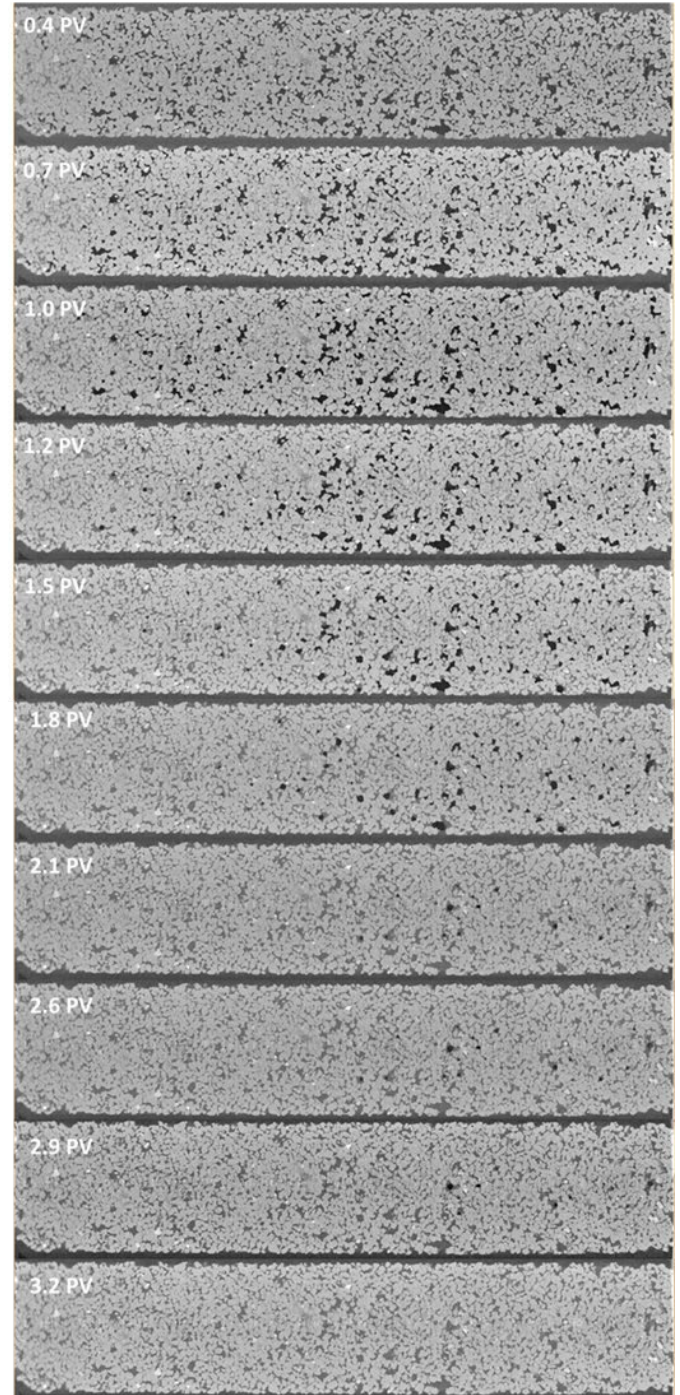
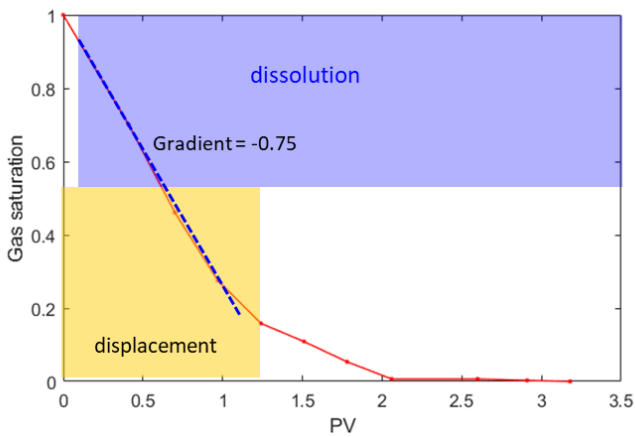


Fig. 9. 2D Grey-scale images perpendicular to the flow direction when the sample was flooded by unsaturated brine. The injection direction is from left to right. Light grey is grain, dark grey is brine, and the black is gas.

Unsaturated Brine



However, for the unsaturated brine case shown in Fig. 12 there are distinct differences compared with the saturated case. At the early stage there is always a superposition of dissolution and displacement. And at the late stage where brine saturation increases above the limit by trapping, i.e. can only increase by dissolution, the dissolution occurs homogeneously over the whole sample, while in the saturated case it was always a frontal dissolution process.

Fig. 10. For the USS flow experiment with unsaturated brine, the red curve shows the trapped gas saturations as a function of pore volumes injected. The yellow shadow represents displacement stage, the purple represents the stage of Dissolution. For unsaturated brine there is a large overlap between displacement and dissolution where dissolution already begins right away in a significant fraction in parallel to displacement processes.

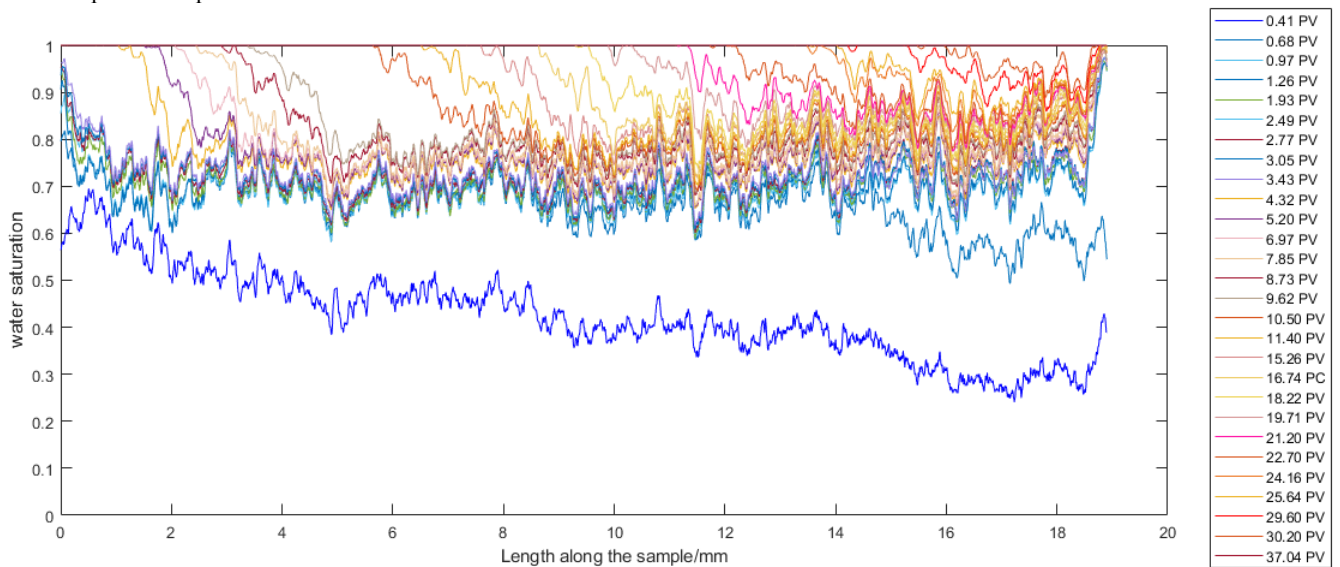


Fig. 11. For the USS flow experiment with gas saturated brine, brine saturation profiles averaged in slices perpendicular to the flow direction at each PV with gas saturated brine injected.

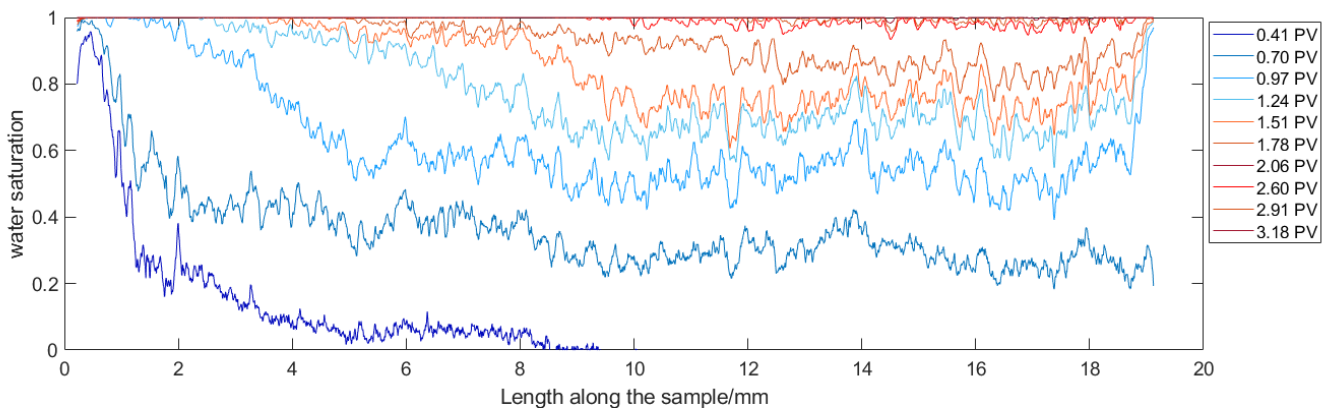


Fig. 12. For the USS flow experiment with unsaturated brine, brine saturation profiles averaged in slices perpendicular to the flow direction at each PV with unsaturated brine injected.

3.4. Trapped gas distribution visualized in 3D

The displacement and dissolution characteristics from the saturation profiles in Section 3.3 are also visible in 3D which allows to visualize also the gas connectivity. Comparing the gas-saturated brine case in Fig. 13 with the unsaturated case in Fig. 14 we found that the gas distribution is very different.

Fig. 13 shows three-dimensional images of the (trapped) gas distribution when it was displaced by *gas-saturated* brine. Each colour represents disconnected gas clusters/ganglia. When 0.4 PV brine was injected, we could see in the gas-saturated brine case the displacement dominated the flow regime and some gas clusters at the inlet start to be isolated while gas volume decreased. When more brine was injected to 0.7 PV, the gas saturated brine has already separated the gas clusters while majority of the gas phase still connected when the similar volume unsaturated brine was flooded. Continually, gas volume decreased with more gas saturated brine injected but gas did not disappear from the inlet of the sample before 7 PV brine was injected.

In other words, the brine passed through the sample first and gas clusters became disconnected first. The dissolution started to play a role after 2 PV brine injected mainly as a frontal dissolution process. During that process, beginning from the inlet side, the volume of each cluster is decreasing gradually until it disappears.

Fig. 14 shows three-dimensional images of the (trapped) gas distribution in the sample when it was displaced by *unsaturated* brine. In general, the volume of disconnected gas cluster/ganglion in Fig. 14 is much smaller and more separated than in the saturated case. The gas decreased much faster and all gas disappeared after injecting around 3 PV brine. However, initially, the gas clusters remain a much higher connectivity in particular towards the outlet indicating that they were not or only very little affected by displacement processes. At the same time, we see already dissolution occurring at the inlet.

Fig. 15 shows an example for the steps how the gas was first trapped and then dissolved in the brine. After 1 PV of gas saturated brine was injected, the gas was trapped in the pore. With more brine was injected, the gas volume is shrinking and gradually becoming a sphere and then eventually disappears completely.

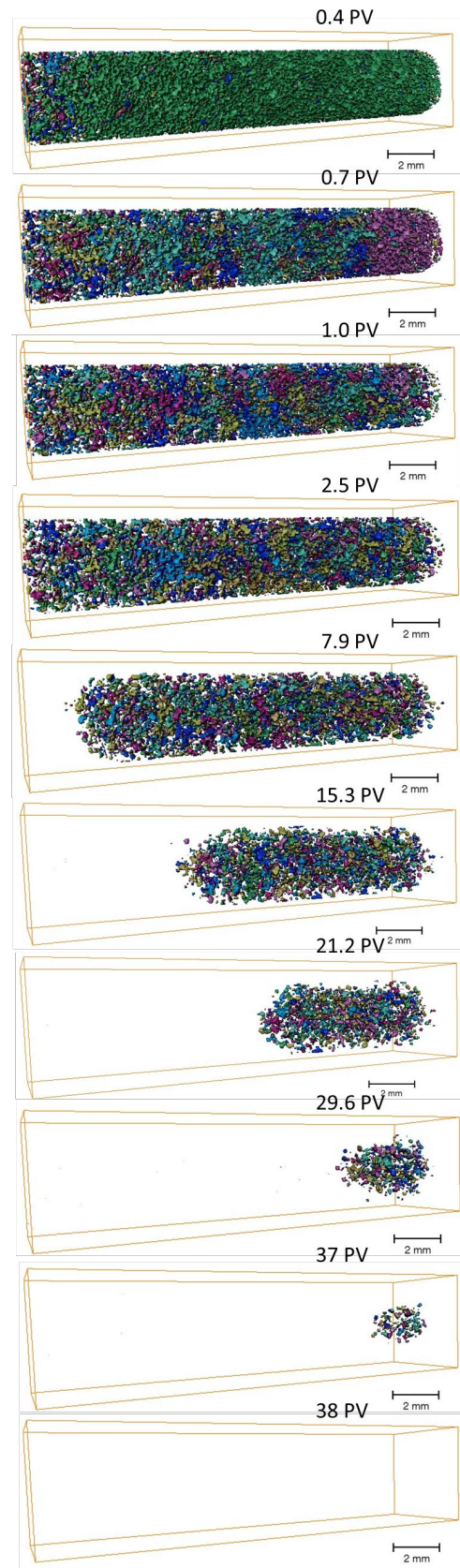


Fig. 13. Three-dimensional images of the configuration of gas along the sample during the USS flow experiment with **gas saturated** brine. Each colour represents separated gas clusters/ganglia.

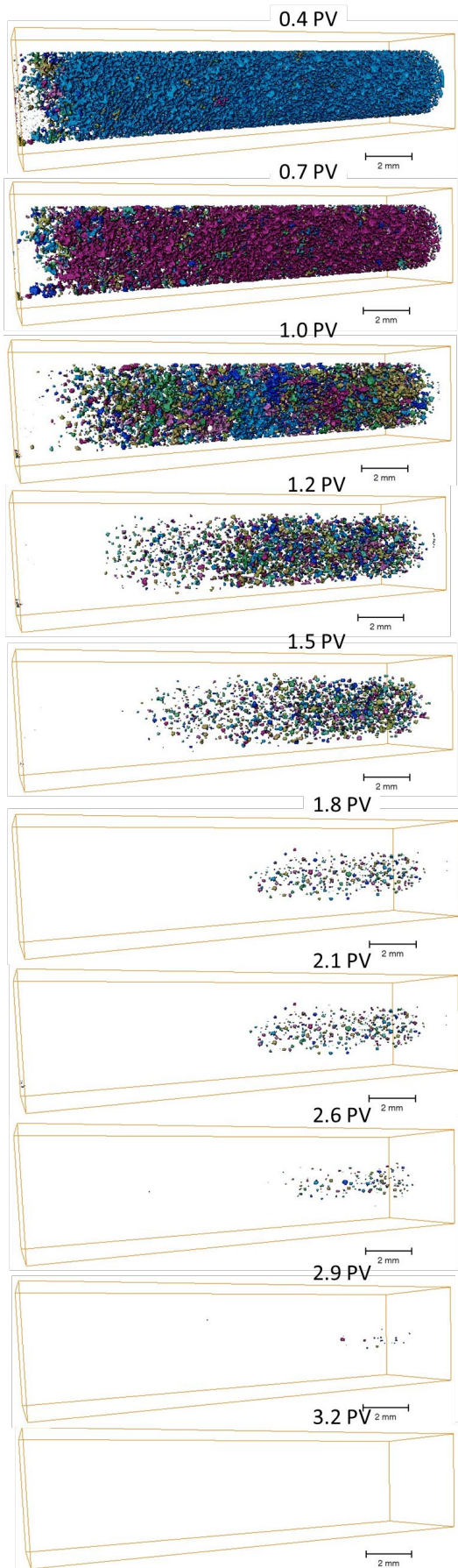


Fig. 14. Three-dimensional images of the configuration of gas along the sample during the USS flow experiment with **unsaturated brine**. Each colour represents separated gas clusters/ganglia.

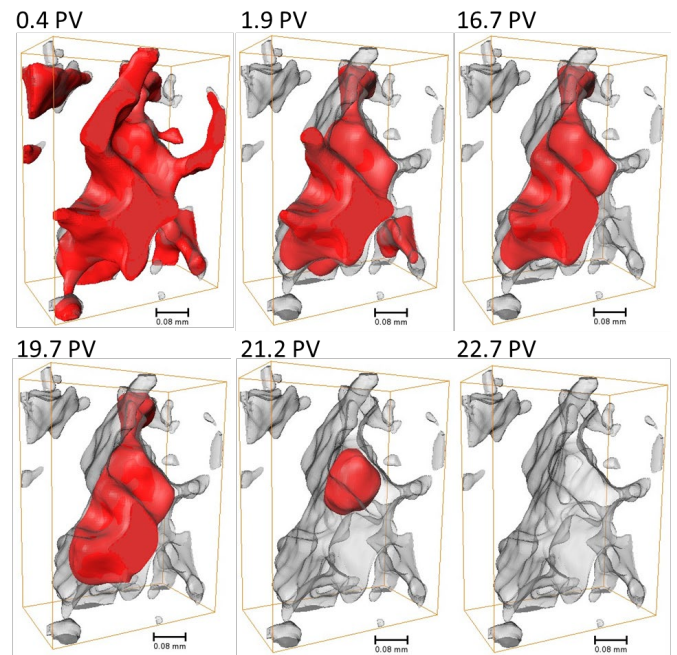


Fig. 15. Gas configuration during injecting at the pore scale. Gas was trapped first and then the volume decreased until disappeared.

That supports the view that the gas-saturated brine must really be at bulk saturation level, i.e. saturation at injection pressure (and temperature). However, in the pore space, that brine is slightly under-saturated with respect to the pore pressure of the gas, which is the injection pressure plus the capillary pressure of the gas. The situation is similar as in ripening dynamics, where local capillary pressure leads to an increase in partitioning of gas into the liquid phase followed by diffusive transport to larger gas bubbles with lower capillary pressure. In absence of external flow, this diffusive exchange leads to the ripening dynamics. As the size of the gas bubble decrease because of the dissolution, the capillary pressure increases which is increasing the dissolution rate.

In previous studies there were already indications for ripening/anti-ripening process occurring in similar situation [45,46,51,52]. This provides a credible setting for the effect observed here as well, only that the situation is slightly different because there is external flow. That means that there is less chance of the traditional ripening to occur where smaller gas bubbles are “eaten” up by larger gas bubbles because that require local super-saturation and diffusive exchange. However, in the presence of an external flow field the advection rate might be locally much higher than diffusion which is then maintaining the concentration at a constant level (saturated to injection pressure at the inlet and due to gas dissolution saturated to a maximum possible saturation throughout the rest of the sample). That prevents the type of mass exchange between smaller and larger bubbles normally seen in Ostwald ripening which is in addition also constrained by pore sizes in porous media.

4 Conclusions

This paper provides fundamentally novel insights into the trapping of gas in sandstone rock, using state-of-the-art imaging techniques during core flooding. An experimental workflow is presented where at the pore scale gas and brine distributions within samples are imaged by 3D X-ray computed micro-tomography, while continuously injecting brine. In contrast to the conventional in-situ saturation monitoring approach, used currently by many SCAL laboratories, this approach has the advantage that the dynamic behaviour of the gas and the changes in saturation are visualized at the pore scale level. This does not only allow us to obtain in situ evidence and to quantification of trapped gas saturation but other impact factors such as capillary effects that may influence the trapping behaviour.

Our experiments reproduce the behaviour reported in the literature [6] that even though gas-saturated brine is injected the trapped gas still dissolves. Without detailed pore scale resolution that allows to discriminate dissolution from displacement at least to some extent, the gas/brine dissolution effect significantly impacts the ability of accurately determining the trapped gas saturation.

By conducting gas trapping flow experiments with both gas-saturated brine and also brine that was not saturated with gas, we could establish a clear difference in pore scale flow regimes between the two situations which differ in dissolution and displacement behaviour. For the non-saturated brine, we observe gas displacement and gas dissolution in parallel, where the gas dissolution follows a predominantly frontal dissolution from the inlet. For the gas-saturated brine, we see a clearer separation of displacement and dissolution processes. Initially the gas saturation decrease is dominated by displacement which leads to disconnected and presumably trapped gas. After almost all gas has been trapped, dissolution occurs more homogeneously throughout the whole sample shrinking first all gas bubbles, followed by a somewhat less pronounced frontal dissolution.

Based on the differences in the displacement/dissolution regime and the observation of the pore scale dissolution dynamics and impact on connectivity, we find supporting evidence that the underlying reason of the dissolution of gas might be linked to ripening dynamics which involves a coupling between phase equilibrium and dissolution/partitioning of components on the one hand and capillarity in the geometric confinement of the pore space on the other hand.

The solution to decrease the impact of dissolution on quantifying trapped gas saturation might be to inject slightly super-saturated brine i.e. brine equilibrated at injection pressure plus a representative capillary pressure, which requires further studies in the future, which are already in the planning.

These insights clearly demonstrate the value of combining multiphase flow experiments with pore-scale imaging because that can provide key insights and lead to solutions to some of the challenges often faced from conventional SCAL experiments. These insights can be used to develop more rigorously validated, physically based pore-scale models of pore scale processes that are more robust than empirical correlations to predict trapped gas saturation under various conditions. For instance, with high quality 3D images of the rock samples with two or three phases flowing through the pore space, how rock structure, flow rate and wettability could impact on the phase behaviours and transport inside of the reservoir subsurface could be clearly captured. The techniques could be adapted for several applications, including EOR, CCS and H₂ storage.

Acknowledgements

The authors would like to thank Rouhi Farajzadeh for very insightful discussions.

References

1. Bachu, S., 2003. Screening and ranking of sedimentary basins for sequestration of CO₂ in geological media in response to climate change. *Environmental Geology*, 44(3), pp.277-289.
2. Benson, S.M. and Cole, D.R., 2008. CO₂ sequestration in deep sedimentary formations. *Elements*, 4(5), pp.325-331.
3. Juanes, R., MacMinn, C.W. and Szulczewski, M.L., 2010. The footprint of the CO₂ plume during carbon dioxide storage in saline aquifers: storage efficiency for capillary trapping at the basin scale. *Transport in porous media*, 82(1), pp.19-30.
4. Blunt, M.J., 2017. *Multiphase flow in permeable media: A pore-scale perspective*. Cambridge university press.
5. Bull, Ø., Bratteli, F., Ringen, J.K., Melhuus, K., Bye, A.L. and Iversen, J.E., 2011, September. The Quest for the True Residual Gas Saturation – an Experimental Approach". In *International Symposium of the Society of Core Analysts*", Texas, USA (pp. 1-12).
6. Cense, A., Reed, J. and Egermann, P., 2016, August. SCAL for gas reservoirs: a contribution for better experiments. In *International Symposium of the Society of Core Analysts held in Snowmass, Colorado, USA* (pp. 21-26).
7. Cense, A.W., Van der Linde, H.A., Brussee, N., Beljaars, J. and Schwing, A., 2014, September. How reliable is in situ saturation monitoring (ISSM) using X-ray?. In *International Symposium of the SCA*.
8. Geistlinger, H., Mohammadian, S., Schlueter, S. and Vogel, H.J., 2014. Quantification of capillary trapping of gas clusters using X - ray microtomography. *Water Resources Research*, 50(5), pp.4514-4529.
9. Herring, A.L., Andersson, L., Schlüter, S., Sheppard, A. and Wildenschild, D., 2015. Efficiently engineering pore-scale processes: The role of force dominance and

- topology during nonwetting phase trapping in porous media. *Advances in Water Resources*, 79, pp.91-102.
10. Gershenzon, N.I., Ritzi Jr, R.W., Dominic, D.F., Mehnert, E., Okwen, R.T. and Patterson, C., 2017. CO₂ trapping in reservoirs with fluvial architecture: Sensitivity to heterogeneity in permeability and constitutive relationship parameters for different rock types. *Journal of Petroleum Science and Engineering*, 155, pp.89-99.
 11. Geffen, T. M., D. R. Parrish, G. W. Haynes, and R. A. Morse. "Efficiency of gas displacement from porous media by liquid flooding." *Journal of Petroleum Technology* 4, no. 02 (1952): 29-38.
 12. Keelan, D.K. and Pugh, V.J., 1975. Trapped-gas saturations in carbonate formations. *Society of Petroleum Engineers Journal*, 15(02), pp.149-160.
 13. Crowell, D.C., Dean, G.W. and Loomis, A.G., 1966. Efficiency of gas displacement from a water-drive reservoir (Vol. 6735). US Department of the Interior, Bureau of Mines.
 14. Pickell, J.J., Swanson, B.F. and Hickman, W.B., 1966. Application of air-mercury and oil-air capillary pressure data in the study of pore structure and fluid distribution. *Society of Petroleum Engineers Journal*, 6(01), pp.55-61.
 15. Land, C.S., 1971. Comparison of calculated with experimental imbibition relative permeability. *Society of Petroleum Engineers Journal*, 11(04), pp.419-425.
 16. Kleppe, J., Delaplace, P., Lenormand, R., Hamon, G. and Chaput, E., 1997, October. Representation of capillary pressure hysteresis in reservoir simulation. In SPE annual technical conference and exhibition. OnePetro.
 17. Suzanne, K., Hamon, G., Billiotte, J. and Trocme, V., 2003, October. Experimental relationships between residual gas saturation and initial gas saturation in heterogeneous sandstone reservoirs. In SPE Annual Technical Conference and Exhibition. OnePetro.
 18. Long, L.C., 1963, June. Experimental research on gas saturation behind the water front in gas reservoirs subjected to water drive. In 6th World Petroleum Congress. OnePetro.
 19. Land, C.S., 1968. Calculation of imbibition relative permeability for two-and three-phase flow from rock properties. *Society of Petroleum Engineers Journal*, 8(02), pp.149-156.
 20. Firoozabadi, A., Olsen, G. and van Golf-Racht, T., 1987, April. Residual gas saturation in water-drive gas reservoirs. In SPE California Regional Meeting. OnePetro.
 21. Holtz, M.H., 2002, April. Residual gas saturation to aquifer influx: A calculation method for 3-D computer reservoir model construction. In SPE Gas Technology Symposium. OnePetro.
 22. Mulyadi, H., Amin, R., Kennaird, T., Bakker, G., Palmer, I., Fletcher, C. and Van Nispen, D., 2000, November. Measurement of residual gas saturation in water-driven gas reservoirs: comparison of various core analysis techniques. In International Oil and Gas Conference and Exhibition in China. OnePetro.
 23. Perrin, J.C. and Benson, S., 2010. An experimental study on the influence of sub-core scale heterogeneities on CO₂ distribution in reservoir rocks. *Transport in porous media*, 82(1), pp.93-109.
 24. Krevor, S.C., Pini, R., Li, B. and Benson, S.M., 2011. Capillary heterogeneity trapping of CO₂ in a sandstone rock at reservoir conditions. *Geophysical Research Letters*, 38(15).
 25. Ni, H., Boon, M., Garing, C. and Benson, S.M., 2019. Predicting CO₂ residual trapping ability based on experimental petrophysical properties for different sandstone types. *International Journal of Greenhouse Gas Control*, 86, pp.158-176.
 26. Blunt, M.J., Bijeljic, B., Dong, H., Gharbi, O., Iglauer, S., Mostaghimi, P., Paluszny, A. and Pentland, C., 2013. Pore-scale imaging and modelling. *Advances in Water resources*, 51, pp.197-216.
 27. Wildenschild, D. and Sheppard, A.P., 2013. X-ray imaging and analysis techniques for quantifying pore-scale structure and processes in subsurface porous medium systems. *Advances in Water resources*, 51, pp.217-246.
 28. Berg, S., Ott, H., Klapp, S.A., Schwing, A., Neiteler, R., Brussee, N., Makurat, A., Leu, L., Enzmann, F., Schwarz, J.O. and Kersten, M., 2013. Real-time 3D imaging of Haines jumps in porous media flow. *Proceedings of the National Academy of Sciences*, 110(10), pp.3755-3759.
 29. Rücker, M., Berg, S., Armstrong, R.T., Georgiadis, A., Ott, H., Schwing, A., Neiteler, R., Brussee, N., Makurat, A., Leu, L. and Wolf, M., 2015. From connected pathway flow to ganglion dynamics. *Geophysical Research Letters*, 42(10), pp.3888-3894.
 30. Berg, S., Armstrong, R., Ott, H., Georgiadis, A., Klapp, S.A., Schwing, A., Neiteler, R., Brussee, N., Makurat, A., Leu, L. and Enzmann, F., 2014. Multiphase flow in porous rock imaged under dynamic flow conditions with fast X-ray computed microtomography. *Petrophysics-The SPWLA Journal of Formation Evaluation and Reservoir Description*, 55(04), pp.304-312.
 31. Spurin, C., Bultreys, T., Bijeljic, B., Blunt, M.J. and Krevor, S., 2019. Mechanisms controlling fluid breakup and reconnection during two-phase flow in porous media. *Physical Review E*, 100(4), p.043115.
 32. Spurin, C., Bultreys, T., Bijeljic, B., Blunt, M.J. and Krevor, S., 2019. Intermittent fluid connectivity during two-phase flow in a heterogeneous carbonate rock. *Physical Review E*, 100(4), p.043103.
 33. Gao, Y., Lin, Q., Bijeljic, B. and Blunt, M.J., 2020. Pore-scale dynamics and the multiphase Darcy law. *Physical Review Fluids*, 5(1), p.013801.
 34. Gao, Y., Raeni, A.Q., Blunt, M.J. and Bijeljic, B., 2021. Dynamic fluid configurations in steady-state two-phase flow in Bentheimer sandstone. *Physical Review E*, 103(1), p.013110.
 35. Al Mansoori, S., Iglauer, S., Pentland, C.H., Bijeljic, B. and Blunt, M.J., 2009. Measurements of non-wetting

- phase trapping applied to carbon dioxide storage. *Energy Procedia*, 1(1), pp.3173-3180.
36. Pentland, C.H., Itsekiri, E., Al Mansoori, S.K., Iglauer, S., Bijeljic, B. and Blunt, M.J., 2010. Measurement of nonwetting-phase trapping in sandpacks. *Spe Journal*, 15(02), pp.274-281.
 37. Bennion, D.B. and Bachu, S., 2010, September. Drainage and imbibition CO₂/brine relative permeability curves at reservoir conditions for carbonate formations. In *SPE Annual Technical Conference and Exhibition*. OnePetro.
 38. Iglauer, S., Wüiling, W., Pentland, C.H., Al-Mansoori, S.K. and Blunt, M.J., 2011. Capillary-trapping capacity of sandstones and sandpacks. *SPE Journal*, 16(04), pp.778-783.
 39. El-Maghraby, R.M. and Blunt, M.J., 2013. Residual CO₂ trapping in Indiana limestone. *Environmental science & technology*, 47(1), pp.227-233.
 40. Khishvand, M., Akbarabadi, M. and Piri, M., 2013. Trapped non-wetting phase clusters: An experimental investigation of dynamic effects at the pore scale using a micro-CT scanner. *SCA*.
 41. Iglauer, S., Paluszny, A., Pentland, C.H. and Blunt, M.J., 2011. Residual CO₂ imaged with X - ray micro - tomography. *Geophysical Research Letters*, 38(21).
 42. Chaudhary, K., Bayani Cardenas, M., Wolfe, W.W., Maisano, J.A., Ketcham, R.A. and Bennett, P.C., 2013. Pore - scale trapping of supercritical CO₂ and the role of grain wettability and shape. *Geophysical Research Letters*, 40(15), pp.3878-3882.
 43. Andrew, M., Bijeljic, B. and Blunt, M., 2014. Reservoir condition pore scale imaging of the capillary trapping of CO₂. *Energy Procedia*, 63, pp.5427-5434.
 44. Andrew, M., Bijeljic, B. and Blunt, M.J., 2014. Pore - by - pore capillary pressure measurements using X - ray microtomography at reservoir conditions: Curvature, snap - off, and remobilization of residual CO₂. *Water Resources Research*, 50(11), pp.8760-8774.
 45. Berg, S., Gao, Y., Georgiadis, A., Brussee, N., Coorn, A., van der Linde, H., Dietderich, J., Alpak, F.O., Eriksen, D., Mooijer-van den Heuvel, M. and Southwick, J., 2020. Determination of critical gas saturation by micro-CT. *Petrophysics-The SPWLA Journal of Formation Evaluation and Reservoir Description*, 61(02), pp.133-150.
 46. Gao, Y., Georgiadis, A., Brussee, N., Coorn, A., van Der Linde, H., Dietderich, J., Alpak, F.O., Eriksen, D., Mooijer-van Den Heuvel, M., Appel, M. and Sorop, T., 2021. Capillarity and phase-mobility of a hydrocarbon gas - liquid system. *Oil & Gas Science and Technology - Revue d' IFP Energies nouvelles*, 76, p.43.
 47. Burger, W. and Burge, M.J., 2016. *Digital image processing: an algorithmic introduction using Java*. Springer.
 48. Benesty, J., Chen, J., Huang, Y. and Cohen, I., 2009. Pearson correlation coefficient. In *Noise reduction in speech processing* (pp. 1-4). Springer, Berlin, Heidelberg.
 49. Buades, A., Coll, B. and Morel, J.M., 2005, June. A non-local algorithm for image denoising. In *2005 IEEE Computer Society Conference on Computer Vision and Pattern Recognition (CVPR'05) (Vol. 2, pp. 60-65)*. IEEE.
 50. Buades, A., Coll, B. and Morel, J.M., 2008. Nonlocal image and movie denoising. *International journal of computer vision*, 76(2), pp.123-139.
 51. Xu, K., Bonnecaze, R. and Balhoff, M., 2017. Egalitarianism among bubbles in porous media: an ostwald ripening derived anticoarsening phenomenon. *Physical review letters*, 119(26), p.264502.
 52. Xu, K., Mehmani, Y., Shang, L. and Xiong, Q., 2019. Gravity - induced bubble ripening in porous media and its impact on capillary trapping stability. *Geophysical Research Letters*, 46(23), pp.13804-13813.